

Experimental and theoretical studies of diamond nucleation on silicon by biased hot filament chemical vapor deposition

B. B. Wang, W. L. Wang,* K. J. Liao, and J. L. Xiao

Department of Applied Physics, College of Science, Chongqing University, Chongqing, 400044, People's Republic of China

(Received 5 April 2000; revised manuscript received 25 July 2000; published 6 February 2001)

Diamond nucleation by biased hot filament chemical vapor deposition was investigated by scanning electron microscopy and atomic force microscopy. It was found that a number of microdefects were produced on a substrate surface owing to energetic ion bombardment under negative substrate bias, which increased with increasing negative bias. The nucleation density was enhanced with an increase of negative bias. During diamond nucleation, a purple glow was observed when the negative bias was increased to a critical value. At the onset of glow discharge, the process of diamond nucleation on a silicon surface by biased hot filament chemical vapor deposition was theoretically studied by analysis of the experimental results of diamond nucleation. The relationship among the number of active ions, the microdefects, and nucleation density with negative bias was given by reasonable analytic formulas. The effect of negative bias on ion diffusion on the substrate surface was theoretically researched and deduced. The influence of negative bias on the bond strength of diamond nuclei on the substrate was analyzed theoretically. The adhesion force between diamond nuclei and the substrate surface was measured by means of the scratch surface method, which was in accord with theoretical consideration. The results indicated that the theoretical calculation was in agreement with experimental results.

DOI: 10.1103/PhysRevB.63.085412

PACS number(s): 81.15.Gh, 81.05.Tp, 68.55.-a, 68.35.Fx

I. INTRODUCTION

Because of its outstanding physical and chemical properties such as high hardness, high temperature resistance, wide optical transmission range, and chemical inertia, diamond is an important strategic material for applications ranging from tribological, thermal, optical, to active electronic applications.^{1,2} Therefore, syntheses of diamond films by chemical vapor deposition (CVD) have attracted enormous interest in the past few decades.^{3,4} The most important step of synthesizing diamond films is diamond nucleation because of its influence on growth rate, morphology, and other qualities of diamond films and their applications.^{5,6} Thus an understanding of diamond nucleation is very important for the growth of diamond films.

Diamond nucleation depends on the substrate materials and is affected by the pretreatment of the substrate surface. To date, silicon has been used as the substrate for deposition of diamond films owing to its low cost and compatibility in electronic device applications. However, few diamond nuclei were nucleated on a mirror-polished substrate surface because of the large lattice mismatch between diamond ($a_0 = 0.3657$ nm) and silicon ($a_0 = 0.5431$ nm), and a much higher surface energy of diamond relative to silicon [6–9 J/m² for diamond (111) surfaces, 1.5 J/m² for silicon (111) surfaces].^{7,8} The nucleation density only reached 10⁴/cm² on the pristine silicon surface.⁹ In order to enhance the nucleation of diamond, the substrate surface was pretreated with diamond powder, deposition of transient layers,^{10–12} ion implantation,¹³ and application of negative substrate bias.¹⁴ The pretreatment of the surface has improved diamond nucleation. Among these methods, negative bias greatly enhanced diamond nucleation, and nucleation density up to 10¹⁰/cm² was achieved on the pristine silicon surface.¹⁴

Many researchers studied nucleation enhancement by negative bias and proposed various mechanisms. Yugo and his colleagues speculated that negative bias increased the hydrogen content of amorphous carbon and the bond strength of diamond nuclei with the substrate.¹⁴ Jiang, Schiffmann, and Klages² claimed that ion bombardment under negative bias increased adatom diffusion. Stoner *et al.*¹⁵ proposed that bias increased the flux of positively charged carbon ions to the surface and that higher energy transferring from ions to the surface resulted in an increased surface mobility of the absorbed species. Robertson *et al.*¹⁶ suggested that ions could be injected into the substrate surface, forming a layer of nanometer graphite, which acts as the transition layer between diamond and substrate. McGinnis, Kelly, and Hagstrom firmly believed that the bombardment of the substrate surface by energetic species was critical for nucleation enhancement.¹⁷ Wang *et al.* indicated that the nucleation density could reach a maximum when negative substrate bias and electron emission simultaneously occurred.¹⁸ Chen and co-workers^{19,20} found that electron emission could enhance diamond nucleation and they believed that electron emission played a key role during diamond nucleation. Wang *et al.*^{21,22} applied a negative bias relative to the filament to the electrode set between the filament and substrate. They found that diamond nucleation was also improved and put forward the mechanism of electron-emission-enhancement (EEE) nucleation. These mechanisms elucidated different aspects of negative-bias-enhanced diamond nucleation.

The mechanisms mentioned above were proposed according to their experimental results, and each of the mechanisms only emphasized some aspects of the enhancement of diamond nucleation by negative bias. Therefore, diamond nucleation has not completely been explained. In fact, diamond nucleation is a complicated process that involves complex physical and chemical processes. It is impossible for

diamond nucleation to be completely explained by a single mechanism. The physical effects of negative bias on diamond nucleation involve ion energy, ion bombardment of the substrate, reactions between ions and the substrate, ion diffusion on a substrate surface, etc.

When negative bias was applied to the substrate, the bias electrical field resulted in an increment of the ionization degree of neutral gas molecules, the energy of ions, and ion bombardment to the substrate surface. It is easily understood that Jiang, Schiffmann, and Klages,² Stoner *et al.*,¹⁵ and Wang *et al.*¹⁸ proposed mechanisms that negative bias and electron emission enhanced diamond nucleation. However, these mechanisms did not take into consideration the effects caused by ion bombardment nor were these mechanisms investigated theoretically. Further research on diamond nucleation under negative bias was restricted.

In the process of diamond nucleation by biased hot filament CVD, a purple glow was observed when the negative bias increased to a critical value,^{7,9} which meant that a glow discharge appeared.²³ At the onset of glow discharge, the physical process of diamond nucleation by biased hot filament CVD was theoretically studied after the phenomena and experimental results were analyzed. The relationship among factors influencing the diamond nucleation was given in some reasonable analytic formulas, and the results of this study were in agreement with the experimental results.

II. EXPERIMENT AND RESULTS

The experiment was carried out in a conventional hot filament CVD system. Mirror-polished $8 \times 8 \text{ mm}^2$ silicon (100) and (111) were used as substrate material. The reaction gas was a mixture of CH_4 and H_2 . The concentration of CH_4 in H_2 ranged from 1% to 3.5%. The total flow of gases was 200 sccm (standard cubic centimeter per minute), which was monitored by a mass flow meter. The total work pressure was $4.0 \times 10^3 \text{ Pa}$. The temperature of the tungsten filament 1 mm in diameter was about $2000 \text{ }^\circ\text{C}$. It was measured by an optical pyrometer. The temperature of the substrate was heated to $850 \text{ }^\circ\text{C}$ by a heater, and it was monitored by a thermocouple, which touched the substrate. The distance between the filament and the substrate was about 8 mm. The negative bias relative to the filament was applied to the substrate through a graphite holder, and the resistance of the bias circuit was larger than $10 \text{ M}\Omega$ to avoid current leakage. The silicon wafer covered the graphite holder completely so that the electronic field could be accumulated on the silicon wafer rather than the holder.

Before nucleation, the silicon wafer was chemically cleaned with acetone and sequential methanol in an ultrasonic bath for 20 min, followed by a 1-min rinse in 50% HF to remove oxide. After the wafer was rinsed with methanol and deionized water again, it was put into the reaction chamber quickly to avoid recontamination. When the chamber was pumped up to a pressure of about 1 Pa, H_2 was fed into the chamber and the tungsten filament was heated to about $2000 \text{ }^\circ\text{C}$. After the wafer was pretreated by H_2 for 5–10 min, CH_4 was fed in. When the temperature of the substrate



FIG. 1. SEM image of diamond nucleation for 35 min without bias.

reached $850 \text{ }^\circ\text{C}$, a negative bias relative to the filament was applied to the substrate, starting the nucleation of diamond.

The process of diamond nucleation was investigated by scanning electron microscopy (SEM) and atomic force microscopy (AFM). The microscopy was operated in the tapping mode by commercial microfabricated silicon cantilevers with a tip diameter of approximately 20 nm. The scanning area ranged from $10 \mu\text{m} \times 1 \mu\text{m}$ to $10 \mu\text{m} \times 10 \mu\text{m}$, and lower scanning areas were used to obtain the image of the pit and the diamond nucleus with very high definition. Figures 1 and 2 show the SEM images of the nucleation of diamond for 35 min without and with negative bias. It is clear that diamond nucleation was greatly enhanced after application of the bias. The nucleation density reached $10^9/\text{cm}^2$ when the bias increased to -250 V , and it increased 5 orders of magnitude compared to that without bias. Experimental results also showed that a number of pits (microdefects) were produced on the substrate surface owing to ion bombardment under negative bias and the diamond nucleus built on the pit. It was found that the number of pits increased with an increase of negative bias.

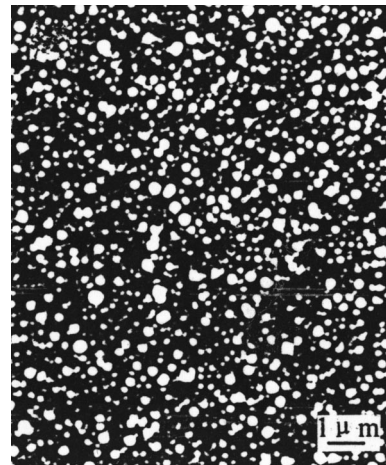


FIG. 2. SEM image of diamond nucleation for 35 min with bias.

III. THEORETICAL ANALYSIS

The experimental results above indicated that diamond nucleation was enhanced with applied negative substrate bias. From the results, it was recognized that bias played an important role in diamond nucleation. In the process of diamond nucleation by biased hot filament CVD, an appreciable current was detected accompanied by a small drop of voltage, and a purple glow was observed when the negative bias relative to the filament applied to the substrate increased to a critical value. This critical value is defined as U_{th} and signals the onset of the emission current or glow. It is related to gaseous pressure, temperature, and distance from the substrate to the filament.^{7,9} This meant that glow discharge appeared and the purple glow was negative glow because the negative glow was bright.²³ It is with the occurrence of the glow discharge that negative bias plays the most important role in diamond nucleation. With the appearance of a glow discharge, a cathode sheath, i.e., the cathode zone from the substrate surface to the edge of the negative glow, builds up near the substrate, and the electrons multiply in the cathode sheath.²⁴ From Ref. 23, it was known that the electrons could collide with gas molecules in the pressure range of 0.1–10 torr. The pressure employed in the process of diamond nucleation generally ranges from 20 to 40 torr; therefore, the electrons would effectively impinge with the gas molecules owing to the fact that the mean free path of electrons was shortened by the increased pressure. The temperature of electrons in H_2 - CH_4 plasma was $(1.0-1.1) \times 10^5$ K,²⁵ i.e., the energy of electrons was 13–14.2 eV. The first ionization energy of CH_4 and H_2 is 12.7 and 13.6 eV,²⁶ respectively. Thus H_2 and CH_4 could be ionized by electron impact to bring about a greater number of ions. The ions obtain energy from the electrical field to strike the substrate surface. Based on the analyses above and the experimental results, it is realized that there are four possible effects that negative bias has on diamond nucleation in the hot filament CVD system: (i) Negative bias increases the flux of active ions. (ii) Negative bias strengthens ion bombardment to the substrate surface, thus resulting in the change of the surface morphology of the substrate and a decrease of the formation energy of the critical nucleus of diamond. (iii) Ion bombardment enhanced by negative bias leads to diffusion enhancement of active ions on the substrate surface. (iv) Ion bombardment strengthened by negative bias enhances the adhesion force between diamond nuclei and substrate. They are discussed in the following.

A. Effect of negative bias on the flux of active ions

As mentioned above, a glow discharge appears when the negative bias relative to the filament applied to the substrate exceeds a critical value. The glow discharge results in the formation of a cathode sheath near the substrate and the production of a number of ions. The cathode sheath observed in the process of diamond nucleation is shown in Fig. 3. In the event of glow discharge, great changes take place in the electrical field owing to space-charge distortion. These changes mainly are concentrated in the cathode sheath so that its field

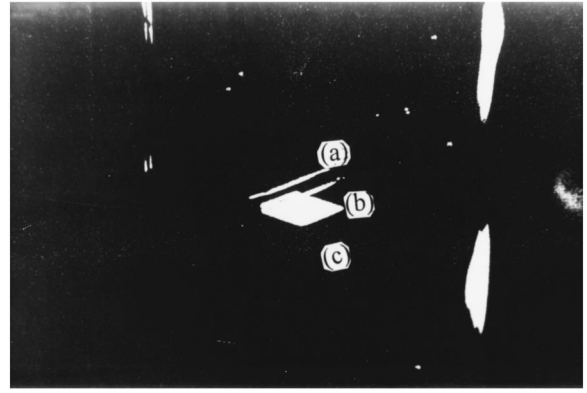


FIG. 3. The cathode sheath: (a) filament, (b) covered plasma sheath near substrate, (c) holder.

becomes highly nonuniform.²³ The highly nonuniform field in the cathode sheath leads to a heterogeneous distribution of ions with the potential. The distribution of ions in the cathode sheath is²⁷

$$\frac{dN}{dU} = \frac{N_0}{2U_c} \frac{L_c}{\lambda} \left(1 - \frac{U}{U_c}\right)^{-1/2} \exp\left\{-\frac{L_c}{\lambda} \left[1 - \left(1 - \frac{U}{U_c}\right)^{1/2}\right]\right\}, \quad (1)$$

where N_0 is the total number of ions entering the cathode sheath from the negative glow and U and U_c are the potential in the sheath and the negative substrate bias relative to the substrate (U_c adopts the absolute value), respectively. λ is the mean free path of active ions in the cathode sheath and L_c is the thickness of the cathode sheath, which depends on the negative bias. Reference 28 indicated that the ion flow to the substrate is mobility limited for the low-pressure range; it is

$$J = C \frac{U_c^2}{L_c^3},$$

where C is constant related to the characteristic of ions. So,

$$L_c = \left(C \frac{U_c^2}{J}\right)^{1/3}.$$

The pressure employed in the process of diamond nucleation is in the low-pressure range. Hence, the relationship between the thickness of the cathode sheath and the negative bias should comply with the ion-mobility-limited current-voltage relationship.

After integration of Eq. (1), the number of ions N_i produced after forming the cathode sheath is

$$N_i = \frac{N_0}{\exp(L_c/\lambda)} \left[\exp\left(\frac{L_c}{\lambda} \sqrt{1 - \frac{U_{th}}{U_c}}\right) - 1 \right]. \quad (2)$$

It is known that when the glow discharge occurs, it is followed by a small collapse of the voltage. However, experiments showed that the purple glow disappeared if the negative bias was reduced to a particular value, the disappearance of the negative glow also meaning the disappearance of glow discharge. Therefore, a minimum voltage is required to maintain the glow discharge. Since N_0 is the number of ions

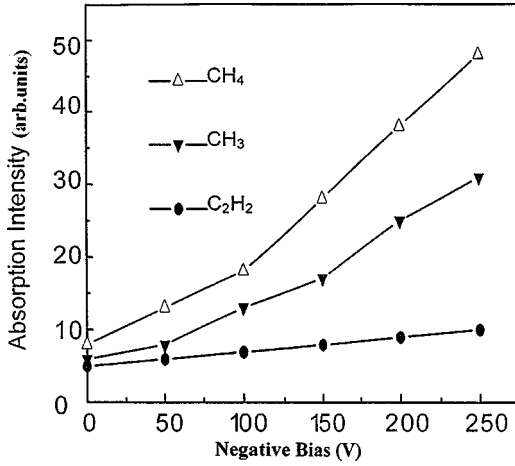
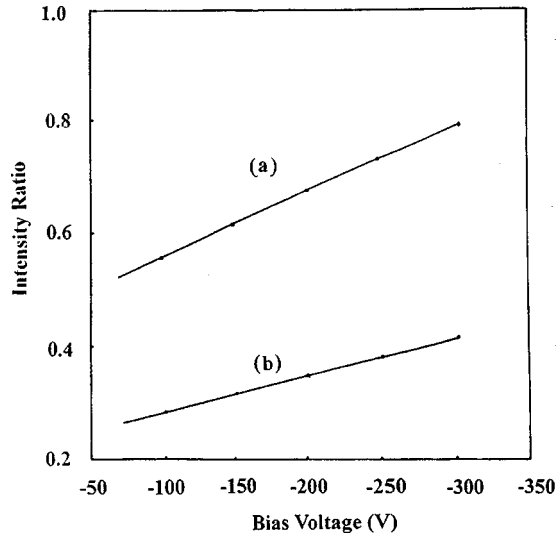


FIG. 4. Absorption intensity vs negative bias.

entering the cathode sheath from the negative glow, U_{th} should be the minimum voltage needed to maintain the negative glow. From Eq. (2), it is obvious that the number of ions increases with increase of negative bias. In order to testify this verdict, in situ infrared absorption (ir) was carried out by placing the reaction chamber into the absorption cell of an infrared spectrometer. Figure 4 shows a variation of ir absorption intensity versus the negative substrate bias near the substrate surface. Apparently, the absorption intensity of CH_3 (606 cm^{-1}) and C_2H_2 (730 cm^{-1}) was enhanced with increasing bias. The ir absorption intensity directly reflects the concentration of adsorbents.^{29,30} Owing to a weak sensitivity to detect ions by ir absorption, the optical emission spectra were used to determine the concentration of the reactive species in the center of the reaction region and vicinity of the substrate surface.³¹ The emission line of Ar at 750 nm was employed as an actinometer.³² Figure 5 shows the optical emission intensity ratio of CH_x (431 nm) and CH_x^+ (422 nm) to Ar (750 nm) as a function of negative bias voltage. It can be seen that the intensity of CH_x and CH_x^+ increased with an

FIG. 5. Emission intensity ratio of CH_x and CH_x^+ as a function of negative bias. (a) CH_x^+ ; (b) CH_x .

increase of bias voltage. This implies that the probability of producing CH_x and CH_x^+ was enhanced with an increase of bias voltage. The experimental results indicated that over 90% of reactive gases were ionized into ions or chemical radicals, but few chemical radicals or ions were created by the heated tungsten filament. Reference 33 indicated that the chemical species produced in CH_4 - H_2 plasma are CH_4^+ , CH_3^+ , CH_2^+ , CH^+ , C^+ , H^+ , H_2^+ , CH_5^+ , and H_3^+ as well as CH_3 , CH_2 , CH , C , and H . It is known that CH_4 is easily ionized into CH_3^+ because the formation energy CH_3^+ is lower than that of producing other ions. References 21 and 22 demonstrated that CH_3^+ takes a critical role in diamond nucleation. Hence, the bias increases the flux of active ions.

B. Influence of ion bombardment on surface morphology of the substrate and formation energy of the critical nucleus of diamond under negative bias

Application of negative bias causes glow discharge and the electrical field mainly concentrates in the cathode sheath. The electrical field is very strong for the majority of voltage drops in the cathode sheath.²³ The active ions obtain energy from the strong electrical field and the energetic ions arrive on the substrate to vigorously bombard the substrate surface.

The energy that an active ion obtains from the sheath is $W = qU$ (q is the ion charge), and the maximum energy of the ion is $W_c = qU_c$. From Eq. (1), the distribution of ions with energy is

$$\frac{dN}{dW} = \frac{N_0}{2W_c} \frac{L_c}{\lambda} \left(1 - \frac{W}{W_c}\right)^{-1/2} \exp\left\{-\frac{L_c}{\lambda} \left[1 - \left(1 - \frac{W}{W_c}\right)^{1/2}\right]\right\}. \quad (3)$$

With integration of Eq. (2), the mean energy of the active ions is

$$\begin{aligned} \langle W \rangle &= \frac{\int_0^{W_c} W \frac{dN}{dW} dW}{\int_0^{W_c} \frac{dN}{dW} dW} \\ &= qU_c \left[\frac{(1 - 2\lambda/L_c) \exp(L_c/\lambda)}{1 - \exp(L_c/\lambda)} + \left(1 - \frac{2\lambda^2}{L_c^2}\right) \right]. \quad (4) \end{aligned}$$

The ratio of electron temperature to ion temperature in plasma, T_e/T_i , is 20–100,²³ so the ion temperature is about 5×10^3 K. The mean free path of CH_3^+ and H^+ is approximately 2.257×10^{-5} and 5.12×10^{-5} m in light of the data in Ref. 26. According to the data in Ref. 18 and the ion-mobility-limited current-voltage relationship,²⁸ the ion energy (current density is 150 mA/cm^2) can be calculated by Eq. (4). The distribution of ion energy versus negative bias is shown in Fig. 6. From Fig. 6, it is known that the ion energy increases with increasing negative bias. The energy of CH_3^+ and H^+ ranges from 55.5 to 143.9 eV and 61.8 to 173.3 eV, respectively, when the negative bias changes from 100 to 300 V, and it is in agreement with experimental results.⁶ The minimum energy of CH_3^+ sputtering silicon is about 38 eV according to the formula³⁴

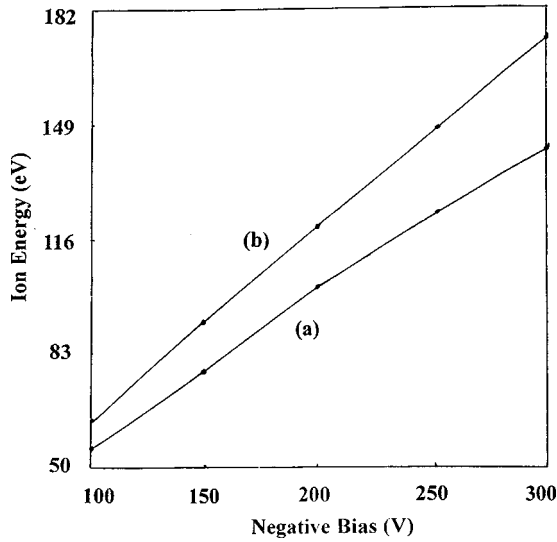


FIG. 6. Distribution of ion energy vs negative bias: (a) energy of CH_3^+ vs negative bias; (b) energy of H^+ vs negative bias.

$$E = 7.7 \frac{(M_i + M_s)^2}{4M_i M_s} W_f,$$

where M_i and M_s are the mass of active ion and silicon atom, respectively, and E and W_f are the ion energy and surface bond energy of silicon, respectively. The energetic CH_3^+ ions strike the silicon substrate and cause the silicon to be sputtered. As a result, microdefects are produced on the silicon surface. Figure 7 shows the surface morphology of the substrate bombarded by ions under negative bias after nucleation for 15 min, after which some diamond nuclei (white points) appear on the pits. The energy of H^+ must reach about 271 eV for the sputtering of silicon to be realized. But the energy of H^+ is 173.3 eV when the negative potential is 300 V, and thus H^+ does not bring about sputtering. Because the negative bias employed in diamond nucleation is usually about 300 V, the energy of active ions falls in a low-energy range. For ions of low energy, the sputtering yield is expressed by³⁵

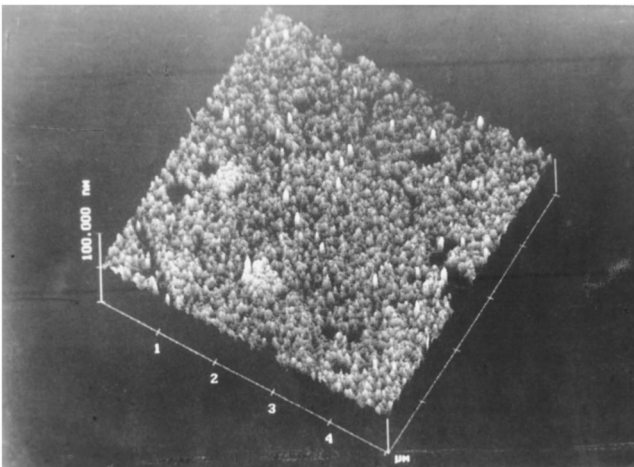


FIG. 7. AFM morphology of substrate surface bombarded by ions under bias (deposition time: 15 min).

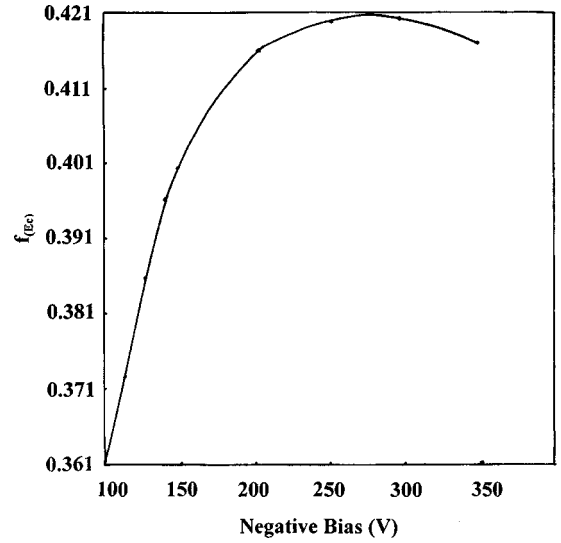


FIG. 8. Relationship curve of $f(E_c)$ vs U_c .

$$S_{(E)} = \frac{3}{4\pi^2} c \frac{4M_i M_s}{(M_i + M_s)^2} \frac{E}{W_f}, \quad (5)$$

where c is a constant related to M_i and M_s , M_i and M_s are the mass of active ion and silicon atom, respectively, and E and W_f are ion energy and surface bond energy of silicon.

From Eq. (3), the sputtering number of silicon by ions is

$$N_1 = \int_{E_{th}}^{E_c} S_{(E)} dN = \frac{3}{4\pi^2} c \frac{4M_i M_s}{(M_i + M_s)^2} \frac{N_0 E_c}{W_f} f(E_c), \quad (6)$$

$$f(E_c) = \frac{1}{\exp(L_c/\lambda)} \left\{ \left[1 - \left(\frac{\lambda}{L_c} \right)^2 - \left(\frac{\lambda}{L_c} - \sqrt{1 - \frac{E_{th}}{E_c}} \right)^2 \right] \times \exp\left(\frac{L_c}{\lambda} \sqrt{1 - \frac{E_{th}}{E_c}} \right) + 2 \left(\frac{\lambda}{L_c} \right)^2 - 1 \right\}, \quad (7)$$

where E_{th} is the threshold energy of ions resulting in the sputtering of silicon. Figure 8 illustrates the relationship of $f(E_c)$ versus U_c ($j = 150 \text{ mA/cm}^2$) and shows that it increases with increasing negative bias, which reaches a maximum value when the negative bias is about 275 V. It is clear that sputtering is strengthened with increasing negative bias and it is predicted that the pit density will have a maximum value with incremental negative bias.

To determine the relationship between the number of pits and negative bias conveniently, it is assumed that ion bombardment produces N_d pits with homogeneous size per unit area of the substrate, as shown in Fig. 9. The volume of a pit

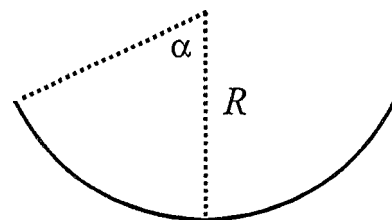


FIG. 9. Shape of a pit.

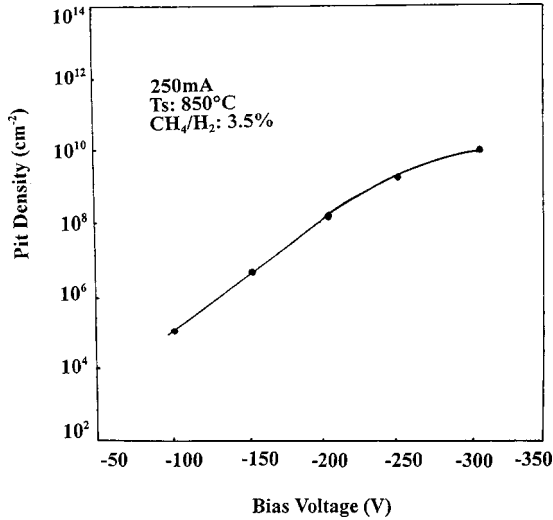


FIG. 10. Relationship curve between the number of pits and bias.

is

$$V_1 = \frac{1}{3} \pi R^3 (1 - \cos \alpha)^2 (2 + \cos \alpha). \quad (8)$$

Given the mass density of silicon ρ , the total mass in N_d pits is

$$m = N_d \rho V_1, \quad (9)$$

and the number of silicon atoms in N_d pits is

$$n = \frac{m}{M} N_A, \quad (10)$$

where M is the molecular mass of silicon and N_A is the Avogadro number. Because the number of silicon atoms in all pits equalizes the number of sputtering silicon atoms, this implies the relationship that n is equal to N_1 . From the equations above, the number of pits per unit area of the substrate surface is

$$N_d = \frac{N_1 M}{\rho N_A} \frac{1}{\frac{1}{3} \pi R^3 (1 - \cos \alpha)^2 (2 + \cos \alpha)}. \quad (11)$$

The experimental results indicated that the size of pits hardly changed with variation of the bias. Equations (6) and (11) indicate that the number of pits increases with increasing negative bias. This is in concordance with experimental result as shown in Fig. 10. From Fig. 10, the pit density tends to a maximum when the negative bias is about 300 V, in accordance with prior predictions

Our experimental evidence showed that diamond nucleates on the pits. George *et al.* found that diamond nuclei built up on the defects.³⁶ So pits play an important role in the process of diamond nucleation. Owing to ion bombardment, the surface morphology of the substrate became roughened and the energy of critical nuclei became varied. Figure 11 shows the nucleus on the pit, which was observed by atomic force microscopy after a deposition of 15 min. From Fig. 11, it is known that the diamond nucleus could be approximated

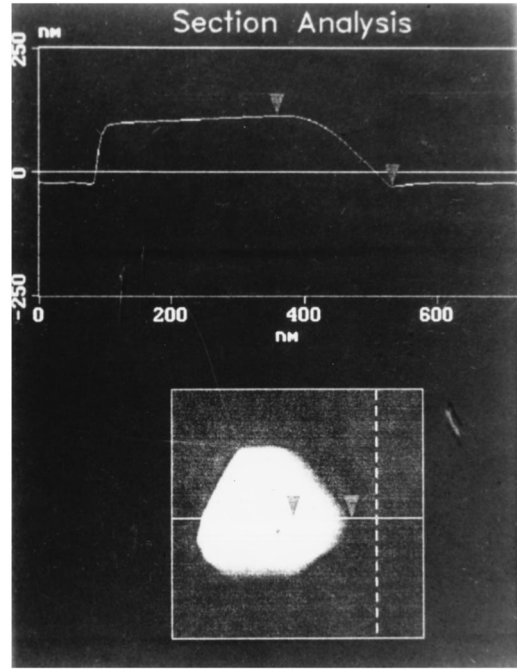


FIG. 11. AFM image of diamond nucleus on pit (deposition time: 15 min).

as a spherical cap. The experimental result showed that the ratio of width to height of diamond nuclei increased with increasing bias as shown in Fig. 12, in which more than 100 particles were measured. This means that the diamond nuclei approach the shape of a spherical cap with an increase of bias; therefore, capillary theory can be applied in diamond nucleation. We assume that a diamond nucleus on a pit takes the form of a spherical cap of radius r , as displayed in Fig. 13. Neglecting the contribution of the system arising from the distribution of adatoms along the possible absorption sites on the surface, we find the formation energy of the nucleus to be

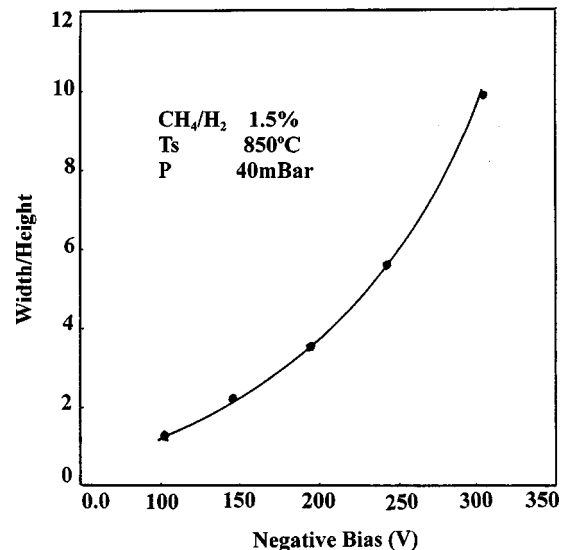


FIG. 12. Diamond nucleus ratio of width to height vs the bias.

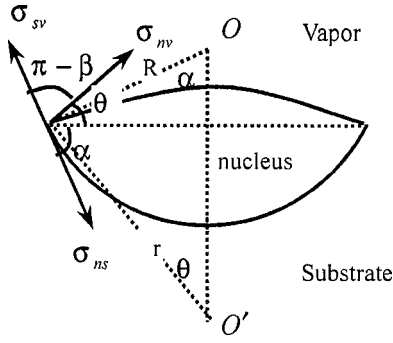


FIG. 13. Nucleus of a spherical cap on the pit.

$$\Delta G = \Delta G_v V + \Delta G_s, \quad (12)$$

where ΔG_v is the supersaturation free energy available per unit volume of the nucleus, ΔG_s is the variation of surface energy after building up the nucleus, and V is the volume of the nucleus. From Fig. 13, the relationship between R and r is

$$R \sin \alpha = r \sin \theta. \quad (13)$$

Before forming the nucleus, the contact area between the gaseous phase and the substrate surface is

$$A_1 = 2\pi R^2(1 - \cos \alpha). \quad (14)$$

The surface area of the spherical cap after forming the nucleus is

$$A_2 = 2\pi r^2(1 - \cos \theta). \quad (15)$$

Therefore, the variation of the surface free energy after building up the nucleus is

$$\Delta G_s = \sigma_{ns}A_1 + \sigma_{nv}A_2 - \sigma_{sv}A_1 = (\sigma_{ns} - \sigma_{sv})A_1 + \sigma_{nv}A_2, \quad (16)$$

where σ_{ns} is the free energy of the interface between substrate and nucleus, σ_{sv} is the free energy of the interface between substrate and vapor, and σ_{nv} is the free energy of the interface between nucleus and vapor. It is noted that the relationship among σ_{ns} , σ_{sv} , and σ_{nv} is

$$\sigma_{sv} = \sigma_{nv} \cos \beta + \sigma_{ns}, \quad (17)$$

where β is the contact angle between the substrate and the vapor, and $\beta = \theta + \alpha$. From Eqs. (14)–(17), ΔG_s becomes

$$\begin{aligned} \Delta G_s &= \sigma_{nv}[2\pi r^2(1 - \cos \theta) - 2\pi R^2(1 - \cos \alpha)\cos \beta] \\ &= \sigma_{nv}2\pi r^2 \left[(1 - \cos \theta) - \frac{\sin^2 \theta}{1 + \cos \alpha} \cos \beta \right]. \end{aligned} \quad (18)$$

The volume of the nucleus is

$$\begin{aligned} V &= \frac{1}{3}\pi r^3(1 - \cos \theta)^2(2 + \cos \theta) \\ &\quad + \frac{1}{3}\pi R^3(1 - \cos \alpha)^2(2 + \cos \alpha) \\ &= \frac{1}{3}\pi r^3 \left[(1 - \cos \theta)^2(2 + \cos \theta) \right. \\ &\quad \left. + (1 - \cos \alpha)^2(2 + \cos \alpha) \frac{\sin^3 \theta}{\sin^3 \alpha} \right]. \end{aligned} \quad (19)$$

Upon the substitution of Eqs. (17) and (19) in Eq. (12), the formation energy of the nucleus is

$$\Delta G = \sigma_{nv}2\pi r^2 f_1 + \Delta G_v \frac{1}{3}\pi r^3 f_2, \quad (20)$$

$$f_1 = (1 - \cos \theta) - \frac{\sin^2 \theta}{1 + \cos \alpha} \cos \beta, \quad (21)$$

$$f_2 = (1 - \cos \theta)^2(2 + \cos \theta) + (1 - \cos \alpha)^2(2 + \cos \alpha) \frac{\sin^3 \theta}{\sin^3 \alpha}. \quad (22)$$

From differentiation of Eq. (20) with respect to r , we can see that the critical radius of the nucleus is

$$r^* = -\frac{4\sigma_{nv}f_1}{\Delta G_v f_2}. \quad (23)$$

Substituting r in Eq. (20) with Eq. (23), the critical energy of building up the nucleus is

$$\Delta G^* = -\frac{1}{6}\Delta G_v \pi r^{*3} f_2. \quad (24)$$

Because the surface area of the substrate taken up by a pit is $S = \pi(R \sin \alpha)^2$, the number of pits on per unit surface of the substrate is also expressed by

$$N_d = \frac{1}{\pi(R \sin \alpha)^2}. \quad (25)$$

From Eqs. (13) and (25), another expression of r^* is found to be

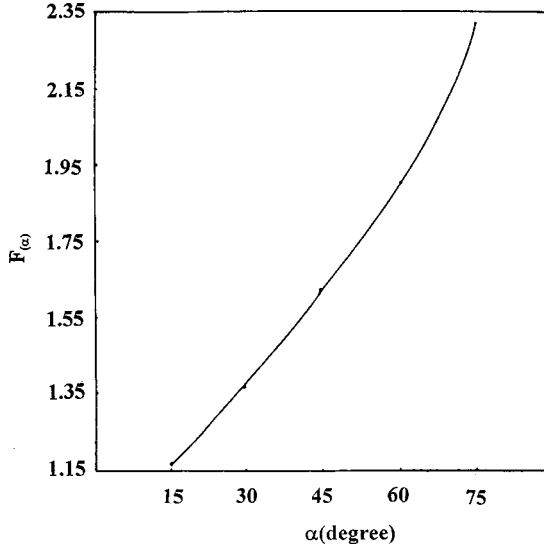
$$r^* = \sqrt{\frac{1}{\pi N_d}} \frac{1}{R \sin \theta}. \quad (26)$$

with substitution of Eqs. (22) and (26) in Eq. (24), the energy of forming the critical nucleus becomes

$$\begin{aligned} \Delta G^* &= -\frac{\pi}{6}\Delta G_v \left(\frac{1}{\pi N_d} \right)^{3/2} \left[\frac{(1 - \cos \theta)(2 + \cos \theta)}{(1 + \cos \theta)\sin \theta} \right. \\ &\quad \left. + \frac{(1 - \cos \alpha)(2 + \cos \alpha)}{(1 + \cos \alpha)\sin \alpha} \right]. \end{aligned} \quad (27)$$

We should note that ΔG_v is negative.

To ensure that Eq. (27) is correct in the course of calculation, let us see Fig. 12 and Eqs. (21)–(24). If $\alpha = 0$ (contact angle, $\beta = \theta$), there are no pits on the substrate surface. From Eqs. (21)–(24), Eq. (24) becomes further

FIG. 14. Relationship curve of $F_{(\alpha)}$ vs α .

$$\Delta G^* = \frac{16\pi\sigma_{nv}^3}{3\Delta G_v^2} \left(\frac{2 - 3\cos\theta + \cos^3\theta}{4} \right). \quad (28)$$

Equation (28) is the critical energy of a nucleus forming on the plane substrate surface.

Let

$$F_{(\alpha)} = \left[\frac{(1 - \cos\theta)(2 + \cos\theta)}{(1 + \cos\theta)\sin\theta} + \frac{(1 - \cos\alpha)(2 + \cos\alpha)}{(1 + \cos\alpha)\sin\alpha} \right]$$

and $\theta = \pi/3$; then the relationship curve of $F_{(\alpha)}$ versus α is shown as in Fig. 14. Figure shows that $F_{(\alpha)}$ is incremental with increasing α and it will further increase when α tends to $\pi/2$. Differentiation of Eq. (27) with respect to N_d gives

$$\begin{aligned} \frac{d\Delta G^*}{dN_d} = & \frac{1}{4}\Delta G_v \left(\frac{1}{\pi} \right)^{3/2} \left(\frac{1}{N_d} \right)^{5/2} \left[\frac{(1 - \cos\theta)(2 + \cos\theta)}{(1 + \cos\theta)\sin\theta} \right. \\ & \left. + \frac{(1 - \cos\alpha)(2 + \cos\alpha)}{(1 + \cos\alpha)\sin\alpha} \right]. \end{aligned}$$

If the angle factor is positive and ΔG_v is negative, $d\Delta G^*/dN_d < 0$, the critical energy for forming a nucleus reduces with pit density. If $\alpha = 0$ or $N_d = 0$, which means that there are no pits on the surface, Eq. (27) is ∞ , which is invalid. The critical energy of forming a nucleus on a plane substrate surface should be calculated by Eq. (28).

On the other hand, from Eq. (18), if α , θ , and β are interrelated as

$$\frac{1 + \cos\theta}{1 + \cos\alpha} \cos\beta > 1, \quad \Delta G_s < 0,$$

which results from the incremental interface area between the substrate and the nucleus, then $\Delta G < 0$ in Eq. (12). Thus, stable diamond nuclei will spontaneously grow, similar to the growth of diamond from its seeds. The above analyses show that the production of pits is significant for diamond nucleation and the pits are nucleation points.

Owing to the application of negative bias, energetic ion bombardment of the substrate produces pits on the surface, which results in an increase of the contact interface between substrate and nuclei. The energy required to build up nuclei reduced, showing that diamond nucleation is enhanced by negative bias.

The nucleation density is expressed by³⁷

$$N_n = N_c \exp\left(-\frac{\Delta G^*}{kT}\right), \quad (29)$$

where N_c is the number of single absorbed atoms per unit area of the substrate surface. From Eqs. (27) and (29) and the analysis above the nucleation density is enhanced with increasing negative bias and has a maximum value since N_d has a maximum value. This trend in line with the experiment results.⁷

C. Ion diffusion enhancement by application of negative bias

Owing to the effect of negative bias, active ions obtain energy from the electrical field, resulting in enhancement of ion bombardment. As a result, in addition to producing the pits, ion bombardment brings about an increase of the substrate temperature, thereby leading to diffusion enhancement of active ions on the silicon surface. In this section, the relationship between diffusion and bias is investigated.

In Sec. III B, the distribution of ions with energy in the cathode sheath was discussed. Based on Eq. (3), similar to calculation of Eq. (6), the total energy of all ions is

$$\begin{aligned} E_t &= \int_0^{E_c} E dN \\ &= \frac{N_0 q U_c}{\exp(L_c/\lambda)} \left[2 \frac{\lambda^2}{L_c^2} - 1 + 2 \left(\frac{\lambda}{L_c} - \frac{\lambda^2}{L_c^2} \right) \exp\left(\frac{L_c}{\lambda}\right) \right]. \end{aligned} \quad (30)$$

In the course of ion bombardment, only a part of the energy is transferred to the substrate surface because part of the ions is reflected. With the assumption that the ratio of the energy transferred to the substrate surface to total energy is g , the energy obtained by the substrate surface is gE_t . The ions whose energy is larger than the threshold value of the sputtering of silicon lead to the sputter, and the number of silicon atoms sputtered is N_1 . But the sputtered silicon atom carries away an energy $\frac{3}{2}kT_s$, where k is Boltzmann's constant and T_s is the temperature of the substrate surface after it is bombarded by ions. Thus the energy that the substrate receives from impingement is

$$E_0 = gE_t - \frac{3}{2}kT_s N_1. \quad (31)$$

If the area over which ions bombard the substrate is A_t and the thickness through which bombarding ions travel is L_s , the number of silicon atoms which that are not sputtered during the impingement process is

$$n = \frac{\rho A_t L_s}{M} N_A - N_1. \quad (32)$$

According to the solid theory,³⁸ the energy of atom is approximately $3kT_s$ at high temperature. The temperature of the silicon substrate was about 1123 K, and it is larger than the Debye temperature, 640 K.³⁹ By energy conservation law, we get the following expression:

$$3kT_0 + \frac{E_0}{n} = 3kT_s, \quad (33)$$

where T_0 is initial temperature of the substrate. From Eqs. (31)–(33), T_s is expressed by

$$T_s = \frac{1}{3k} \frac{gE_t - \frac{3}{2}kT_0N_1}{(\rho A_t L_s / M)N_A - \frac{1}{2}N_1} + T_0. \quad (34)$$

The diffusion coefficient of active ions on the substrate surface is

$$D = a^2 \nu_i \exp\left(-\frac{E_d}{kT_s}\right), \quad (35)$$

where E_d is the active energy of ion diffusion, ν_i is the vibration frequency of ions, and a is the distance between the two positions of nucleation.

Based on collision theory,⁴⁰ each H^+ ion loses about 5% of its energy after it impinged on the silicon atom, i.e., each H^+ ion gives the silicon substrate an energy of several eV because H^+ has over 100 eV (see Fig. 6). From Sec. III B, CH_3^+ ions mainly cause silicon sputter, but the number of CH_3^+ ions is rather lower than the number of H^+ ions since their density was only 1%–3.5%. Therefore H^+ ions mainly cause the increase of the silicon surface temperature. It is well known that sputter depends on the ion mass: the larger the ion mass, the higher the sputter yield. The sputter yield of silicon by Ar^+ bombardment is from 0.11 to 0.18 when its energy changes from 100 to 200 eV.⁴¹ For CH_3^+ , the sputter yield should be lower than the preceding values because its mass is less than the mass of Ar^+ . Then, according to the current-voltage relationship given in Sec. III A, Fig. 6, and Eq. (34), the change of substrate surface temperature with bias is shown in Fig. 15(a). Figure 15(a) shows that the surface temperature increased from 850 to 948 °C when the bias was raised from 0 to 250 V, in agreement with experimental results [Fig. 15(b)]. From Eq. (35), the diffusion coefficient increases exponentially with temperature, and ion diffusion on the substrate surface is greatly enhanced.

Analyses indicate $gE_t > \frac{3}{2}kT_0$ when $T_0 = 1123$ K, and Eq. (34) becomes

$$T_s = \frac{1}{3k} \frac{gE_t - 0.15N_1}{(\rho A_t L_s / M)N_A - \frac{1}{2}N_1} + T_0. \quad (36)$$

From Eq. (36), the temperature of the substrate surface increases with increasing N_1 , and it will reduce when N_1 increases to a particular value. From differentiation of Eq. (34) with respect to N_1 ,

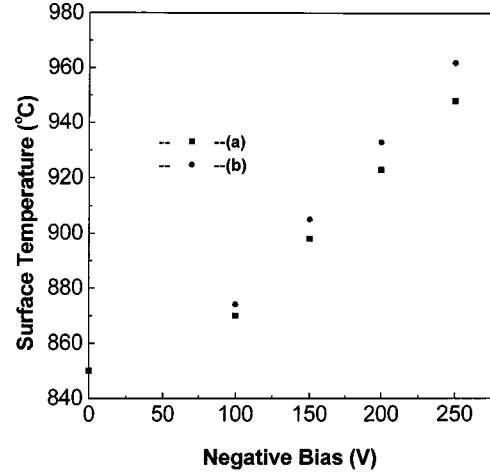


FIG. 15. Relationship curve between T_s with negative bias: (a) theoretical results; (b) experimental results.

$$\frac{dT_s}{dN_1} = \frac{1}{6k} \frac{gE_t - 3(\rho A_t L_s / M)N_A k T_0}{[(\rho A_t L_s / M)N_A k - \frac{1}{2}kN_1]^2}. \quad (37)$$

If Eq. (37) = 0, then

$$E_t = \frac{3}{g} kT_0 \frac{\rho A_t L_s}{M} N_A. \quad (38)$$

When Eq. (38) holds true, the surface temperature can attain the highest value. Generally, the sputter time is shorter and the sputter yield is low, and therefore Eq. (38) does not hold. As a result, T_s increases with increasing N_1 so that ion diffusion on the surface is improved by negative bias.

In addition, the increase of the substrate temperature can result in the formation of an amorphous structure.⁴² Therefore, it is inevitable that there are amorphous structures in diamond films. A number of experiments have demonstrated amorphous structures created during diamond nucleation.^{43–46}

D. Influence of negative bias on the adhesion force between diamond nuclei and the substrate

In the experimental results mentioned above, it is known that diamond nucleation is enhanced under application of negative bias. This implies that the adhesion force between diamond nuclei and the substrate is enhanced. A lot of experiments showed that silicon carbide was formed in the process of diamond nucleation.^{2,15,47} Silicon carbide has two effects during diamond nucleation. First, silicon carbide acts as a transient layer between the substrate and diamond films because it reduces the mismatch of lattice constant between diamond and silicon as the lattice constant of silicon carbide lies between diamond and silicon. Second, silicon carbide strengthens the adhesion force between diamond nuclei and the substrate. Reference 42 shows that the atoms of the substrate undergo displacement due to incidental ion bombardment when the energy of incidental active ions reaches the threshold value of displacement of the substrate atoms, and the incidental ions interact with the displaced substrate at-

oms. Simultaneously, Refs. 42 and 48 also indicate that a compound layer on the substrate surface results in enhancement of the bond strength of the film on the substrate. In the process of growing diamond films, the compound is silicon carbide. According to Kujinov's theory,⁴⁹ the adhesion force between diamond nuclei and the substrate, F , is proportional to the amount of interaction between incident ions and silicon, N_{int} :

$$F \propto N_{\text{int}}. \quad (39)$$

The amount of interaction between incidental ions and silicon atoms includes the amount of silicon carbide (silicon atoms) with which the incidental ions directly react and the amount of silicon carbide deposited on the substrate surface again after the sputtered silicon atoms react with ion in the gaseous phase. We assume that the threshold value of the displacement of a silicon atom is E_p and the minimum energy of incidental ions causing displacement of a silicon atom is E_m . According to the collision theory,³⁶ the energy that the silicon atom obtains from the process of impingement is

$$E_s = E \frac{4M_i M_s}{(M_i + M_s)^2} \cos^2 \phi, \quad (40)$$

where ϕ is the scattering angle of the silicon atom after it is impinged. The maximum energy that the silicon atom receives is

$$E_{sm} = E \frac{4M_i M_s}{(M_i + M_s)^2}. \quad (41)$$

From this formula, the minimum energy of ion leading to the displacement of silicon atoms is

$$E_m = E_p \frac{(M_i + M_s)^2}{4M_i M_s}. \quad (42)$$

Incidental ions interact with displaced silicon atoms and form silicon carbide. The amount of this silicon carbide is

$$N_2 = \int_{E_m}^{E_{\text{th}}} dN = \frac{N_0}{\exp(L_c/\lambda)} \left\{ \exp\left[\frac{L_c}{\lambda} \sqrt{1 - \frac{E_p}{E_c} \frac{(M_i + M_s)^2}{4M_i M_s}}\right] - \exp\left(\frac{L_c}{\lambda} \sqrt{1 - \frac{E_{\text{th}}}{E_c}}\right) \right\}. \quad (43)$$

When the energy of incidental ions is larger than the threshold value of sputtering of silicon, the number of sputtered silicon atoms is N_1 , and some of the sputtered silicon atoms take part in the reaction with incidental ions. Provided the ratio is p , then the amount of the interacting silicon is

$$N_3 = pN_1 \quad (44)$$

and the total amount of silicon carbide is

$$N_{\text{int}} = N_2 + N_3. \quad (45)$$

From Eqs. (6) and (43)–(45), F is expressed by

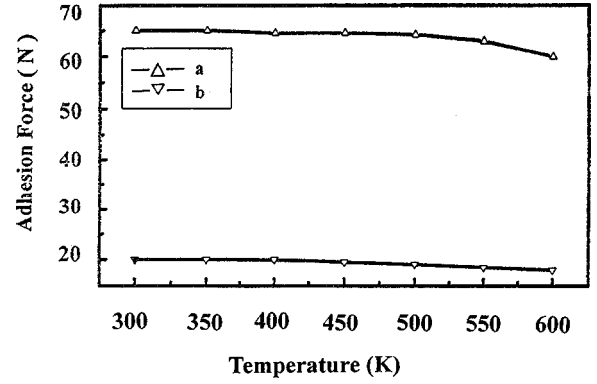


FIG. 16. The adhesion force between diamond film and WC substrate vs temperature, (a) with bias pretreatment; (b) without bias.

$$F \propto \frac{N_0}{\exp(L_c/\lambda)} \left\{ \exp\left[\frac{L_c}{\lambda} \sqrt{1 - \frac{E_p}{E_c} \frac{(M_i + M_s)^2}{4M_i M_s}}\right] - \exp\left(\frac{L_c}{\lambda} \sqrt{1 - \frac{E_{\text{th}}}{E_c}}\right) \right\} + p \frac{3}{4\pi^2 c} \frac{4M_i M_s}{(M_i + M_s)^2} \frac{N_0 E_c}{W_f} f(E_c). \quad (46)$$

From Eqs. (7) and (46), it is obvious that the adhesion force between diamond nuclei and the substrate is strengthened with increasing negative bias. This conclusion is in accord with the experimental result. The adhesion force between diamond films and the WC substrate was measured by the method of the scratch test, which is similar to that of Ref. 50. The results are shown in Fig. 16, which shows the adhesion force between diamond films and WC substrate with temperature. From the figure, it can be seen that the adhesion force was found to be higher than 60 N with bias treatment [see Fig. 16(a)], but was lower than 20 N without bias [see Fig. 16(b)].

E. Heteroepitaxial growth of diamond by substrate negative bias

Substrate bias pretreatment not only led to a high nucleation density of diamond on untreated silicon substrate but was also a crucial step in growing heteroepitaxial diamond films.^{22,51–53} Figure 11 shows the threefold symmetry of the diamond particle after 15 min deposition, which suggests a (111) silicon orientation of the crystal. The diamond particle was grown on a p -type (111) silicon substrate under a bias pretreatment of 15 min. From the AFM surface image, it is known that the crystallite is (111) textured with a (111)-oriented silicon substrate, i.e., diamond (111) \parallel Si(111) plus diamond $\langle 1\bar{1}0 \rangle \parallel \text{Si} \langle 1\bar{1}0 \rangle$ for (111). However, the role of negative bias in the heteroepitaxial nucleation of diamond has given rise to controversy.

In fact, the epitaxial growth mode in a given system depends on interfacial free energy and lattice mismatch. In general, heteroepitaxial growth is best achieved by Frank–Van der Merwe⁵⁴ layer-by-layer growth. But, the higher surface energy of diamond relative to silicon favors island formation of diamond on silicon (VM mode) and local epitaxial growth

due to the large lattice mismatch between diamond and silicon. The bias pretreatment plays two important roles in the heteroepitaxial nucleation. First, ion bombardment of the substrate under negative bias greatly decreases the formation energy of diamond on silicon substrate (see Sec. III B). Second, the contact area of nuclei with the substrate increases with the negative-bias voltage (see Fig. 11). On the other hand, studies based on semiempirical molecular orbital calculations and molecular mechanics have shown that it is possible to grow oriented textured diamond films on a Si(111) surface.^{55,56}

IV. SUMMARY

In summary, the process of diamond nucleation was theoretically investigated. The results showed that negative bias played an important role in the process of diamond nucleation in the hot filament CVD system and indicated that the negative bias enhanced the number of active ions. Simultaneously, it reduced the formation energy of critical nuclei of diamond owing to the production of pits by ion bombardment and improved ion diffusion enhancement on the substrate surface due to the increase of the substrate surface temperature by ion bombardment under negative bias. The negative bias also strengthened the bond strength of diamond nuclei on the substrate surface. These are all key factors that influence diamond nucleation. Therefore, diamond nucleation is enhanced by negative bias in a hot filament CVD system.

ACKNOWLEDGMENT

The work was financially supported by the National Natural Science Foundation of China under Grant No. 19904016.

APPENDIX: CALCULATION OF EQS. (6) AND (7)

From Eqs. (1) and (5), we get

$$N_1 = \int_{E_{th}}^{E_c} S_{(E)} dN = \int_{E_{th}}^{E_c} \frac{3}{4\pi^2} c \frac{4M_i M_s}{(M_i + M_s)^2} \frac{E}{W_f} \frac{N_0}{2E_c} \frac{L_c}{\lambda} \times \left(1 - \frac{E}{E_c}\right)^{-1/2} \exp\left[-\frac{L_c}{\lambda} \left[1 - \left(1 - \frac{E}{E_c}\right)^{1/2}\right]\right] dE \\ = \frac{3}{4\pi^2} c \frac{4M_i M_s}{(M_i + M_s)^2} \frac{N_0 E_c}{W_f \exp(L_c/\lambda)} \int_{E_{th}}^{E_c} \frac{E}{E_c} \frac{L_c}{2\lambda} \times \left(1 - \frac{E}{E_c}\right)^{-1/2} \exp\left[\frac{L_c}{\lambda} \left(1 - \frac{E}{E_c}\right)^{1/2}\right] d\left(\frac{E}{E_c}\right). \quad (A1)$$

Let

$$f_{(E_c)} = \frac{1}{\exp(L_c/\lambda)} \int_{E_{th}}^{E_c} \frac{E}{E_c} \frac{L_c}{2\lambda} \left(1 - \frac{E}{E_c}\right)^{-1/2} \times \exp\left[\frac{L_c}{\lambda} \left(1 - \frac{E}{E_c}\right)^{1/2}\right] d\left(\frac{E}{E_c}\right), \quad (A2)$$

$x = E/E_c$, and $x_1 = E_{th}/E_c$, then Eq. (A2) becomes

$$f_{(E_c)} = \frac{1}{\exp(L_c/\lambda)} \int_{x_1}^1 x \frac{L_c}{2\lambda} (1-x)^{-1/2} \exp\left[\frac{L_c}{\lambda} (1-x)^{1/2}\right] dx. \quad (A3)$$

In Eq. (A3), let $t = (1-x)^{1/2}$ and $t_1 = (1-x_1)^{1/2}$, then Eq. (A3) is expressed by

$$f_{(E_c)} = \frac{1}{\exp(L_c/\lambda)} \int_0^{t_1} (1-t)^2 \exp\left(\frac{L_c}{\lambda} t\right) d\left(\frac{L_c}{\lambda} t\right). \quad (A4)$$

After integration of Eq. (A4), $f_{(E_c)}$ is expressed by [Eq. (7)]

$$f_{(E_c)} = \frac{1}{\exp(L_c/\lambda)} \left\{ \left[1 - \left(\frac{\lambda}{L_c}\right)^2 - \left(\frac{\lambda}{L_c} - \sqrt{1 - \frac{E_{th}}{E_c}}\right)^2 \right] \times \exp\left(\frac{L_c}{\lambda} \sqrt{1 - \frac{E_{th}}{E_c}}\right) + 2 \left(\frac{\lambda}{L_c}\right)^2 - 1 \right\}$$

and Eq. (A1) becomes [Eq. (6)]

$$N_1 = \frac{3}{4\pi^2} c \frac{4M_i M_s}{(M_i + M_s)^2} \frac{N_0 E_c}{W_f} f_{(E_c)}.$$

*Author to whom correspondence should be addressed. FAX: +86 23 65106704. Email address: wanluw@cqu.edu.cn

¹W. L. Wang, K. J. Liao, B. Feng, G. Sanchez, M. C. Polo, and J. Esteve, *Diamond Relat. Mater.* **7**, 528 (1998).

²X. Jiang, K. Schifmann, and C.-P. Klages, *Phys. Rev. B* **50**, 8402 (1994).

³W. L. Wang, K. J. Liao, and B. B. Wang, *J. Mater. Sci. Technol.* **16**, 19 (2000).

⁴R. Samlenski, G. Flenig, R. Brenn, C. Wild, W. Muller-Sebert, and P. Koidl, *J. Appl. Phys.* **74**, 2134 (1993).

⁵J. B. Cui and R. C. Fang, *Appl. Phys. Lett.* **69**, 3507 (1996).

⁶Sz. Katai, Z. Tass, Gy. Hars, and P. Deak (unpublished).

⁷W. L. Wang, G. Sanchez, M. C. Polo, R. Q. Zhang, and J. Esteve, *Appl. Phys. A: Mater. Sci. Process.* **65**, 241 (1997).

⁸W. L. Wang, M. C. Polo, G. Sanchez, J. Cifre, and J. Esteve, *J. Appl. Phys.* **80**, 1846 (1996).

⁹W. Zhu, F. R. Sivazlian, B. R. Stoner, and J. T. Glass, *J. Mater. Res.* **10**, 425 (1995).

¹⁰T. Hartnett, R. Miller, D. Montanari, C. Willingham, and R. Tustison, *J. Vac. Sci. Technol. A* **8**, 2129 (1990).

¹¹Z. M. Yu, T. Rogelet, and S. A. Flodstrom, *J. Appl. Phys.* **74**, 7235 (1993).

¹²S. D. Wolter, B. R. Stoner, J. T. Glass, P. J. Eillis, D. S. Buhaenko, C. E. Jenkins, and P. Southworth, *Appl. Phys. Lett.* **62**, 1215 (1993).

¹³Jie Yang, Xiaowei Su, Qijin Chen, and Zhangda Lin, *Appl. Phys. Lett.* **66**, 3284 (1995).

¹⁴S. Yugo, T. Kanai, T. Kimura, and T. Muto, *Appl. Phys. Lett.* **58**, 1036 (1991).

¹⁵B. R. Stoner, G.-H. M. Ma, S. D. Wolter, and J. T. Glass, *Phys. Rev. B* **45**, 11 067 (1992).

¹⁶J. Robertson, J. Gerber, S. Sattel, M. Weiler, K. Jung, and H.

- Ehrhardt, Appl. Phys. Lett. **66**, 3287 (1995).
- ¹⁷S. P. McGinnis, M. K. Kelly, and S. B. Hagstrom, Appl. Phys. Lett. **66**, 3117 (1995).
- ¹⁸W. L. Wang, K. J. Liao, Z. G. Zhang, and M. Y. Liao, Acta. Phys. Sin. **6**, 517 (1997).
- ¹⁹Qijin Chen, Jie Yang, and Zhangda Lin, Appl. Phys. Lett. **67**, 1853 (1995).
- ²⁰Qijin Chen and Zhangda Lin, Appl. Phys. Lett. **68**, 2450 (1996).
- ²¹W. L. Wang, K. J. Liao, J. Wang, L. Fang, P. D. Ding, J. Esteve, M. C. Polo, and G. Sanchez, Diamond Relat. Mater. **8**, 123 (1999).
- ²²W. L. Wang, K. J. Liao, B. Feng, and Z. Zhang, Chin. Phys. Lett. **15**, 460 (1998).
- ²³Herman V. Boenig, *Plasma Science and Technology* (Cornell University Press, Ithaca, 1982), Chaps. 2 and 3.
- ²⁴Thomas C. Paulick, J. Appl. Phys. **67**, 2774 (1990).
- ²⁵K. Suzuki, A. Sawabe, and T. Inuzuka, Appl. Phys. Lett. **53**, 1818 (1988).
- ²⁶Koosai Konuma (Japan), *Film Deposition by Plasma Techniques*, translated by G. H. Zhang (in Chinese) (National Defense Industry, Beijing, 1994), Chap. 2.
- ²⁷S. Maniv, W. D. Westwood, and P. J. Scanlon, J. Appl. Phys. **53**, 856 (1982).
- ²⁸J. H. Ingold, in *Gaseous Electronics* (Academic, New York, 1978), Vol. 1, Chap. 2.
- ²⁹F. G. Cell, P. E. Pehrsson, H.-T. Wang, and J. E. Butler, Appl. Phys. Lett. **52**, 2043 (1988).
- ³⁰Jib-Jen Wu and Franklin Chau-Nan Hong, Appl. Phys. Lett. **70**, 185 (1997).
- ³¹H. Barankova and L. Bardos, Diamond Relat. Mater. **2**, 347 (1993).
- ³²J. W. Coburn and M. Chen, J. Appl. Phys. **51**, 3134 (1980).
- ³³Minoru Tsuda, Mitsuo Nakajima, and Setsuko Oikawa, J. Am. Chem. Soc. **108**, 5780 (1986).
- ³⁴Lishi Wen, *Physical Basis of Study on Interface of Solid Materials* (Academic, Beijing, China, 1991), p. 264.
- ³⁵P. Sigmund, Phys. Rev. **184**, 383 (1969).
- ³⁶M. A. George, A. Burger, W. E. Collins, J. L. Davidson, A. V. Barnes, and N. H. Tolk, J. Appl. Phys. **76**, 4099 (1994).
- ³⁷T. N. Rhodin and D. Walton, *Metal Surface: Structure, Energetics and Kinetics* (American Society for Metals, Metal Park, Ohio, 1963), p. 272.
- ³⁸J. S. Blakemore, *Solid State Physics*, 2nd ed. (Cambridge University Press, London, 1985), p. 122.
- ³⁹Syuuichi Mesida *et al.* (Japan), *Handbook of Physics Constants*, translated by Z. X. Zhang (Academic, Beijing, China, 1979), p. 91.
- ⁴⁰Daming Sun and Guangkang Xi, *Surface and Interface of Solids* (Anhui Education Press, Hefei, China, 1996), p. 438.
- ⁴¹Bangzhao Yang and Wensheng Wang, *Film Physics and Technology* (Electron Science and Technology University Press, Chengdu, China, 1994), p. 69.
- ⁴²Tonghe Zhang, Yuguang Wu, *Optimum Technology of Ion Implantation Surface* (Metallurgy Industry Press, Beijing, China, 1993), p. 210.
- ⁴³Y. Liao, R. C. Feng, F. Ye, Q. Y. Shao, and G. Z. Wang, Mod. Phys. Lett. B **13**, 159 (1999).
- ⁴⁴W. L. Wang, K. J. Liao, and B. B. Wang, Proc. SPIE **3862**, 479 (1999).
- ⁴⁵M. Kawavada, K. Kurihara, K. Sasaki, A. Teshima, and K. Koshino, Proc. SPIE **1146**, 28 (1989).
- ⁴⁶R. G. Buckley, T. D. Moustakas, Ling Ye, and J. Varon, J. Appl. Phys. **66**, 3595 (1989).
- ⁴⁷M. C. Polo, J. Cifre, and J. Esteve, Diamond Relat. Mater. **3**, 492 (1994).
- ⁴⁸Dunyi Tang, Shuquan Lin, and Zhimin Liou, *Technology and Application of Strong Flux of Charged Particle Beam* (Electron Industry Press, Beijing, China, 1995), pp. 173–189.
- ⁴⁹B. B. Kujinov (Russia), *Plasma Coat*, translated by Lishi Wen, Xuguang Ming, and Xiaofeng Chen (Science Press, Beijing, China, 1981), p. 97.
- ⁵⁰J. R. Frerericck and K. C. Ludema, J. Appl. Phys. **35**, 256 (1964).
- ⁵¹X. Jiang, C.-P. Klages, R. Zachai, M. Hartweg, and H.-J. Fusser, Appl. Phys. Lett. **62**, 3438 (1993).
- ⁵²B. R. Stoner and J. T. Glass, Appl. Phys. Lett. **62**, 698 (1992).
- ⁵³Y. K. Kim, K. Y. Lee, and J. Y. Lee, Appl. Phys. Lett. **68**, 756 (1996).
- ⁵⁴F. C. Frank and J. H. Van der Merwe, Proc. R. Soc. London, Ser. A **198**, 205 (1949).
- ⁵⁵R. Q. Zhang, W. L. Wang, J. Esteve, and E. Bertran, Appl. Phys. Lett. **69**, 1086 (1996).
- ⁵⁶R. Q. Zhang, W. L. Wang, J. Esteve, and E. Bertran, Thin Solid Films **317**, 6 (1998).